Valence shell electronically excited states of imidazole and 1-methylimidazole

D.M.P. Holland, D.A. Shaw, D. Townsend, I. Powis

Published version information

Citation: D. M. P. Holland, D. A. Shaw, D. Townsend & I. Powis (2023) Valence shell electronically excited states of imidazole and 1-methylimidazole, Molecular Physics, 121:7-8,

DOI: https://doi.org/10.1080/00268976.2022.2122614

This is an Accepted Manuscript of an article published by Taylor & Francis in Molecular Physics on 22. 09. 2022,

available at: https://doi.org/10.1080/00268976.2022.2122614."

Valence shell electronically excited states of imidazole and 1-methylimidazole

D. M. P. Holland[a], D. A. Shaw[a], D. Townsend[b,c] and I. Powis[d]

[a] Daresbury Laboratory, Daresbury, Warrington, Cheshire WA4 4AD, United Kingdom

[b] Institute of Photonics and Quantum Sciences, Heriot-Watt University, EH14 4AS, United Kingdom

[c] Institute of Chemical Sciences, Heriot-Watt University, EH14 4AS, United Kingdom

[d] School of Chemistry, The University of Nottingham, University Park, Nottingham NG7 2RD, United Kingdom

ABSTRACT

The absolute photoabsorption cross section of imidazole, and that of 1-methylimidazole, have been measured from threshold up to 10.8 eV using synchrotron radiation. For each molecule, the absorption spectrum exhibits several broad bands due to transitions into excited valence states and some sharp structure associated with Rydberg states. Assignments have been proposed for some of the observed absorption bands using calculated transition energies and oscillator strengths. Quantum defects have also helped guide these assignments. Natural transition orbital plots indicate that many of the electronically excited states have a mixed Rydberg/valence character. This mixing leads to irregularities in both the transition energies and the relative intensities of the absorption bands ascribed to Rydberg states. The vibrational progressions belonging to some of the Rydberg states have been interpreted using simulations of the corresponding cation's vibrational structure obtained within the Franck-Condon model employing harmonic frequencies and normal modes.

Keywords: imidazole photoabsorption spectrum; excited valence and Rydberg states; quantum defects; Natural Transition Orbitals

Contact: D M P Holland email david.holland@stfc.ac.uk

1. Introduction

The valence shell vertical excitation spectrum of imidazole ($C_3H_4N_2$, Figure 1) has been studied extensively [1-6] with most of the attention being focussed on the $\pi \rightarrow \pi^*$, $\pi \rightarrow \sigma^*$, $n \rightarrow \pi^*$ and $n \rightarrow \sigma^*$ transitions. Indeed, imidazole was selected as one of the molecules on which to perform benchmark calculations of vertical excitation energies and oscillator strengths for electronically excited states using a variety of computational methods [4]. Although these theoretical investigations have improved our understanding of the low energy valence transitions, very little information is available concerning transitions into Rydberg states.

The main obstacle in assessing the theoretical predictions for the excited state transition energies and oscillator strengths is the lack of a gas phase absolute photoabsorption cross section. Devine et al. [7] have measured a relative photoabsorption spectrum of gaseous imidazole in the excitation range ~4.9 – 6.5 eV. Based upon previously reported theoretical predictions for imidazole, and by analogy with the spectrum of the closely related pyrrole molecule, a weak absorption band observed in that spectrum at low photon energies was associated with the $\pi(3a'') \rightarrow 3s(a')$ transition, and the more intense absorption at energies above ~5.6 eV was attributed to one or more $\pi \rightarrow \pi^*$ transitions [7]. The UV absorption spectrum of aqueous imidazole has also been recorded and exhibits two broad bands with maxima around 6.0 and 6.5 eV [8,9]. Although the peak position and the relative intensity of the band observed around 6.0 eV do not vary significantly with changes in the solvation conditions, variations were observed for the band appearing at higher excitation energy [8].

Serrano-Andrés et al. [3] employed the complete active space, self-consistent field method and multireference second-order perturbation theory to study the valence shell electronic spectrum of gaseous imidazole. Solvation effects were also investigated. The results predicted that the most intense absorption bands should arise from the $\pi \rightarrow \pi^*$ excitations but, in addition, significant oscillator strengths were calculated for several transitions into Rydberg states. More recent theoretical investigations [4-6] have concentrated on transitions into the σ^*

and π* valence orbitals with the only Rydberg transition included in the calculations being that due to the 3a″ → 3s excitation.

Imidazole has also been chosen to test recent developments in non-adiabatic dynamics simulations of ultrafast relaxation processes following UV excitation [10]. The decay dynamics of UV excited imidazole have been investigated in several time-resolved, pump-probe experiments [5-7, 10-12] but the interpretation of these results has been hampered by the incomplete knowledge of the neutral excited states populated by the pump photon.

Imidazole has a planar (C_s) five-membered heteroaromatic ring structure and its valence shell photoelectron spectrum has been studied recently, both experimentally and theoretically, by Patanen et al. [13]. Calculations showed that the highest occupied molecular orbital in the neutral ground state is 3a″, but the energies of the next two occupied orbitals (2a″ and 15a′) were predicted to be very similar to each other, and the energetic ordering of these two orbitals was found to depend sensitively upon the computational method employed. The non-bonding 15a′ orbital may be considered as a σ-type lone-pair located on the N_3 atom (Figure 1) [13]. In addition to the two occupied π-orbitals (3a″ and 2a″), imidazole possesses two low-lying virtual π* orbitals. Vibronic coupling may be affecting the valence ionic states of imidazole [13].

In the present work, the absolute photoabsorption cross section of imidazole, and that of 1-methylimidazole ($C_4H_6N_2$, Figure 2), have been measured from their onset up to an energy of 10.8 eV. Several computational approaches have been employed to calculate vertical transition energies and oscillator strengths for excited valence and Rydberg states. These theoretical predictions have guided the assignments proposed for the observed absorption bands. Identification of the specific character of the calculated excitations is aided by visual examination of the Natural Transition Orbitals (NTOs) [14-16] that, following transformation of the canonical orbitals, provide a simplified representation of the excitations as one-electron transitions between an initial and final orbital.

Extensive vibrational structure appears in the absorption spectra associated with transitions into some of the Rydberg states. Franck-Condon simulations of the vibrational spectra due to transitions into the ground ionic states of imidazole and 1-methylimidazole were calculated using harmonic frequencies and normal modes. These vibrational simulations, together with those measured previously for imidazole [13], provided useful information in the identification of bands arising from transitions into Rydberg states. In addition, a threshold photoelectron spectrum of 1-methylimidazole is reported.

2. Experimental apparatus and procedure

2.1. Absolute photoabsorption cross sections

The absolute photoabsorption cross sections of imidazole and 1-methylimidazole were measured using a cell incorporating LiF windows [17] and synchrotron radiation emitted from the Daresbury Laboratory storage ring [18]. The cell was attached to a 5 m normal incidence monochromator which delivers radiation in the energy range of ~5 – 45 eV [19]. In the present experiment a photon resolution of 0.1 nm FWHM (~5 meV at hν = 8 eV) was employed.

The photoabsorption cross section was obtained through application of the Beer-lambert law:

$$I_t = I_0 \exp\left(-n\sigma l\right) \qquad (1)$$

where I_t is the intensity of the transmitted radiation after passing through the gas column, I_0 is the corresponding incident intensity, n is the gas number density, σ is the absorption cross section, and l is the length of the gas column. The spectrum of imidazole was recorded at a temperature of 60°C, resulting in a sample pressure of 15 μbar, whilst that of 1-methylimidazole was recorded at a temperature of 45°C, resulting in a sample pressure of 10 μbar. These slightly elevated above-ambient temperatures are unlikely to significantly degrade the recorded detail, and indeed we estimate that a much greater degree of *cooling* would be required before observing a significant improvement in the thermal congestion present in the spectrum. The experimental uncertainty associated with the determination of absolute photoabsorption cross

sections using this cell is estimated as ~5% [17]. The photon energy scale was calibrated by recording high resolution absorption spectra of a gas mixture comprising imidazole (1-methylimidazole), nitrous oxide and nitric oxide [20].

2.1. Threshold photoelectron spectrum

The threshold photoelectron spectrum of 1-methylimidazole was recorded in the energy range 8 – 19 eV using the electron detection part of an electron-ion coincidence spectrometer [21,22], attached to the same monochromator as used in the absorption measurements. The spectrum was normalised to variations in the incident photon intensity using the signal from a photomultiplier located behind the interaction region. The monochromator resolution was set at 0.1 nm FWHM (~18 meV at hν = 15 eV). The energy scale was calibrated by recording a threshold photoelectron spectrum of a gas mixture comprising 1-methylimidazole, argon and xenon. Lithium fluoride or indium filters could be inserted into the photon beam exiting the monochromator to help suppress higher order radiation.

3. Computational details

3.1. Excited state vertical transition energies and oscillator strengths

The principal excited state calculations were performed with the Gaussian 16 [23] and QChem 5.0 [24] packages using time-dependent density functional theory (TD-DFT). The reliable estimation of Rydberg excited states requires use of a range-separated functional, and for this we use the CAM-B3LYP functional with a d-Aug-cc-pVTZ basis. Alternatively, a hybrid basis (which we designate cc-pVTZ+R5p5) consisting of unaugmented cc-pVTZ functions on atomic centres with a large set of diffuse Rydberg-like functions placed at the molecular centre-of-mass was used. For the latter, we used the prescription of Kaufmann et al. [25] to generate a set of s, p, d, and f Rydberg-like functions ranging up to n = 5½ (n = 4½ for f). For the low-lying Rydberg states (3p and below) the two basis sets yield nearly identical results. For both molecules, the starting geometries for the ground state were obtained from MP2/cc-pVTZ optimisations. In the calculations, the z-axis is set normal to the molecular plane, while the y

axis is arbitrarily defined to be perpendicular to the line between positions 1 and 5 and passing through position 3 (Figure 1).

The identification/characterisation of the excited states was aided by use of the one particle density matrix (OPDM) analysis provided in QChem [15,16,24] to examine the transition induced change in electron density. Each excitation is then characterised by the corresponding electron-hole pair, with the OPDM electron size indicating the spatial extent of the excited electron. The identification of the specific character of the calculated states is further assisted by visual examination of the NTOs [14-16] that provide the simplest one-particle representation of an excitation using unitary transformations of the occupied and virtual canonical orbitals.

3.2. Outer valence Green's function calculations

Vertical ionisation energies were estimated by Outer Valence Green's Function (OVGF) calculations using Gaussian 16 [23] with a cc-pVTZ basis.

3.3. Franck-Condon simulations of cation vibrational spectra

Harmonic vibrational analyses for frequencies and normal modes were performed for the ground state neutral and ground state cation of either molecule using B3LYP/cc-pVTZ and MP2/cc-pVTZ calculations. The numbering of the vibrational modes follows the nomenclature recommended by Herzberg [26]. Franck-Condon simulations of the vibrational structure in the cation photoelectron spectrum (and by implication in the excitation spectra to pure Rydberg states – vide infra) were then prepared. Franck-Condon factors were then calculated using the adiabatic hessian model, including Duschinsky rotations, provided in Gaussian 16 [21], and convoluted with a 240 cm^{-1} FWHM Gaussian shaping function to generate realistic spectral profiles.

In the case of 1-methylimidazole, the lowest frequency found ($\leq$ 77 cm^{-1}) for both ion and neutral can be assigned as a methyl torsional mode. This is likely far from harmonic in character, and in fact the B3LYP calculation for the cation reports the frequency to be imaginary, indicating a failure to locate a true potential minimum for this mode. Such a low

frequency oscillation is, in any case, unlikely to contribute anything other than an underlying continuum to an experimental spectrum recorded with the present resolution. Hence, given the uncertainties, this low frequency oscillation has been omitted from the full simulations.

4. Results and discussion

4.1 Overview

The absolute photoabsorption cross sections of imidazole and 1-methylimidazole, across the full energy range covered in the present experiment, are plotted in Figure 3. The threshold regions are shown in greater detail in Figure S1 (Supplementary Information). In each molecule, the absorption spectrum exhibits prominent sharp structure superimposed upon a continuum containing several very broad bands. All of the sharp absorption bands will be shown to arise from transitions in Rydberg states, with the underlying broad features attributed to valence states.

A common, traditionally adopted procedure to help identify absorption bands associated with Rydberg states is to consider the quantum defect of that band, through use of the formula:

$$E_n = E_\infty - 13.606 \Big/ \left(n - \delta_l\right)^2 \qquad (2)$$

where E_n is the transition energy for the promotion of an electron from a particular orbital into a Rydberg orbital of principal number n, E_∞ is the relevant ionisation energy, and δ_l is the quantum defect for the lth series. For a given value of l (the orbital angular momentum), δ_l generally lies within a small range and is almost independent of n for an unperturbed series. Typically, δ_l lies within the ranges (0.8 to 1.0), (0.4 to 0.7), and (– 0.2 to +0.2) for ns, np and nd series, respectively. For isolated Rydberg states, assignments based upon quantum defect considerations work well. However, if a Rydberg state is perturbed through interactions with an adjacent valence state, then the transition energy may be shifted from that predicted by Eq (2) and the oscillator strength may be affected. Under such circumstances, the excited states may no-longer be described adequately in terms of a predominantly one-electron excited

configuration, but rather possess a mixed Rydberg/valence character. Regular Rydberg series may not be observed when mixing occurs.

Table 1 summaries the properties of the excited states of imidazole derived from our calculations. We use {} brackets, together with an included number, to denote a specific state listed in Table 1. The symmetry, the orbital from which the transition originates, the calculated transition energy, and the oscillator strength are listed for each state together with an assessment of the Rydberg and/or valence character of the final orbital obtained from visual inspection of the principal NTO plot for the excitation. The excited state characterisation is further supported by three columns providing numerical indicators of the spatial extent or size of the excited state or orbital. The first of these compares the conventional $<R_\chi^2>$ expectation value (actually the second cartesian moment of the electron density) of the excited state, χ, relative to that of the ground state. One may anticipate that $<R_\chi^2>$ values for a pure Rydberg state will significantly exceed those obtained for a valence state. Considering, for example, states {1}–{5} in Table 1, it is readily seen from their $\Delta<R_\chi^2>$ values that states {2},{3}and{4} are significantly more extensive than states {1} and {5}, whose values are barely increased from those of the ground state, thus confirming a significant Rydberg character for states {2}–{4}. Conversely, states {1} and {5} display a similar size to the ground state and so must share with it a dominantly valence character. By the same token, the rather greater extent of states {2} and {4} (assigned as the $3p_x$ and $3p_y$ states) as compared to the $3p_z$ state {3}, suggests that symmetry allowed $3p_z$ coupling with the π^* orbitals may result in a more strongly mixed Rydberg/valence character for the latter.

The density matrix analysis provides values for R_e, the size of the excited electron orbital, and $D_{e\text{-}h}$, the RMS electron–hole separation. Noting that the majority of the transitions originate from the same 3a″ orbital, and hence that the 'hole' radius is effectively invariant, it is perhaps not surprising that trends in R_e and $D_{e\text{-}h}$ very closely parallel one another. Indeed, the same trends are apparent in these density matrix estimators of the excited electron size, and the $\Delta<R_\chi^2>$ estimators of the final state size, whose interpretation hence appears to be

corroborative. As noted above, a more diffuse character identified by the increasing size of any of these measures can usefully aid an assessment of the Rydberg character of a given state.

Similar information concerning the excited states of 1-methylimidazole, their spatial extents and assignments is given in Table 2.

In imidazole and 1-methylimidazole, many of the absorption bands associated with Rydberg states display accompanying vibrational structure. Since the molecular geometry of a Rydberg state is generally similar to that of the ionic state onto which the series converges, the Franck-Condon factors connecting the ground and Rydberg state are expected to be similar to those connecting the ground and corresponding ionic state. Thus, the assignments for the vibrational structure appearing in the photoabsorption spectrum may be guided through comparison with those for the associated photoelectron band.

The interpretation and proposed assignments of the structure observed in the experimental absorption spectra of imidazole and 1-methylimidazole are based on our calculated transition energies and oscillator strengths, and the information provided by viewing the NTOs. For Rydberg states, the quantum defects and the comparison between the observed and simulated vibrational progressions are also taken into account. In practice, the theoretical results provide reliable assignments for the low-lying excited states but become more sensitive to the details of the calculations with increasing excitation energy. Thus, at higher energies, quantum defects are employed to predict the occurrence of Rydberg states.

4.2. Photoabsorption spectrum of imidazole

Our calculations predict that the lowest energy singlet excited state {1} is due to a transition from the 3a″ orbital into an orbital having a mixed σ_{NH}* valence and 3s(a′) Rydberg character. The inner valence ring density associated with state {1} is visually apparent in Figure 4, enclosed within the spatially much larger Rydberg 3s contribution. This A″ state, with a calculated vertical transition energy of 5.515 eV and an oscillator strength of 0.0007, does not appear to give rise to a distinct feature in the experimental spectrum. Instead, the absorption

cross section gradually increases from an onset around 5.4 eV to reach a plateau value of ~20 Mb at 6 eV (Figure 3).

In the energy region between 6.2 and 6.9 eV, some sharp structure superimposed upon a significant continuous intensity appears in the experimental absorption spectrum (Figure 5(a)). This structure, as discussed below, resembles that observed in the $X\ ^2A''$ state photoelectron band [13]. Use of the Rydberg formula (Eq (2)), and the experimental ionisation energy of 8.842 eV for the 3a″ orbital [13], results in a quantum defect of 0.705 for the absorption band at 6.258 eV. A quantum defect of this value is typical of a p-type state.

The second and third predicted states (Table 1) have similar calculated transition energies in this region and both possess a mixed valence/Rydberg character. State {2} is predicted at 6.259 eV, with an oscillator strength of 0.0241, and is due to a transition from the 3a″ orbital into an orbital having σ_{CH}* (and possibly some σ_{NH}*) valence character, together with $3p_x$ Rydberg character. State {3} is predicted at 6.267 eV, with a much larger oscillator strength of 0.1415, and is due to a transition from the same 3a″ orbital into an orbital possessing a $3p_z$ Rydberg character (Figure 4), borrowing intensity from its more strongly mixed $\pi_{C\text{-}C\text{-}N}$* valence component. At slightly higher energy, the 3a″ → $3p_y$ A″ transition is predicted at 6.493 eV (state {4}) but with a very low oscillator strength (Table 1).

Taking into consideration the oscillator strengths, it seems reasonable to ascribe the sharp absorption bands occurring between 6.2 and 6.9 eV to a single Rydberg state {3}, due to the 3a″ → $3p_z$ A′ transition.

The $X\ ^2A''$ state photoelectron band of imidazole has been discussed in detail by Patanen et al. [13]. A comparison between the experimental and the simulated spectra indicated that the principal peaks were due to excitations involving the ν_7^+ and ν_{12}^+ modes, either alone or in various combinations with each other. In addition, smaller contributions arose from excitation of the ν_{14}^+ mode, either alone or in combination with the ν_7^+ and ν_{12}^+ modes. The experimentally derived vibrational energies for the ν_7^+ and ν_{12}^+ modes were 170 and 124 meV, respectively.

For convenience, the FC simulation of the $(3a'')^{-1}$ X $^2A''$ state [13], with the principal vibrational excitations labelled, is plotted in Figure 5(b). Overall, the simulation reproduces the main features appearing in the absorption spectrum, particularly in the lower energy region. In the higher energy region, the observed absorption peaks are broader than predicted for the ionic state, perhaps indicating additional rapid decay mechanisms available for the neutral state [6,11,12]. Table 3 lists the excitation energies and proposed assignments of the structure observed in the absorption spectrum due to the $3a'' \rightarrow 3p_z$ A' transition. The absorption spectrum allows vibrational energies of 169, 129 and 113 meV to be derived for the ν_7, ν_{12} and ν_{14} modes, respectively, using the bands in the Rydberg state around 6.3 eV. Our calculated (B3LYP/cc-pVTZ) energies for the ν_7, ν_{12} and ν_{14} modes in the neutral (ionic) ground state (Table S1), after applying an appropriate harmonic scaling of 0.968 [27], are 172 (170), 131(125) and 114(111) meV, respectively. In comparison, the measured values in the neutral ground state are 174.4, 134.5 and 114.7 meV, respectively [28].

The results from the present work provide an explanation for the solvation-dependent peak positions and relative intensity variations observed previously [8] in the two broad bands occurring around 6.0 and 6.5 eV. Figures 3 and 5(a) show that the band around 6.5 eV would have contained a significant contribution from transitions into a Rydberg state whereas that around 6.0 eV is predominantly due to a valence state. Owing to the anticipated larger spatial size of a Rydberg state compared to that of a compact valence state, solvation conditions are known to affect Rydberg state absorption bands to a greater degree [29]. Thus, the large change in the peak position and intensity of the higher energy band is consistent with the Rydberg nature of the state.

In the energy range 6.0 to 7.3 eV, the experimental absorption spectrum seems to consist of a continuum, having a value of ~20 Mb, together with the prominent bands due to the $3a'' \rightarrow 3p_z$ Rydberg excitation discussed above. Our calculations predict various states in this region (states {5}–{10}, excluding state {7}) which contain some valence character. Note that states {5} and {10} involve transitions from the 15a′ and 2a″ orbitals, respectively, whereas states

{6}, {8} and {9} involve excitation from the 3a″ orbital. It appears reasonable to attribute the valence contributions associated with these states to the observed underlying continuum intensity.

The absorption cross section (Figure 6) exhibits a distinct increase around 7.3 eV and, in the region between 7.3 and 9.0 eV, contains extensive, complex structure due to transitions into Rydberg states belonging to series converging onto the $X\ ^2$A″ state ionisation limit. The high absorption cross section, and the width of the band maximum upon which the sharp structure due to the Rydberg states is superimposed, suggest that this region also contains numerous valence states. Our theoretical results are consistent with this interpretation although ascribing predicted valence states to observed broad features is not feasible.

We use the absorption bands observed between 6.2 and 7.0 eV, probably due to transitions into a single Rydberg state, as a model in attempting to assign the complicated structure appearing at energies above 7.3 eV. Two sharp peaks are observed at 7.326 and 7.416 eV, both of which are likely to be associated with the adiabatic transitions into Rydberg states. In both states, the three most prominent peaks due to transitions into vibrationally excited levels can also be identified. The quantum defects derived from the peaks at 7.326 and 7.416 eV, tentatively associated with adiabatic transitions, are 0.004 and –0.089 for $n = 3$, respectively. These quantum defects suggest that both Rydberg states should be assigned as 3d. It is also conceivable that the peak observed at 7.567 eV arises for the adiabatic transition into another 3d state.

According to our theoretical results, state {7}, with a calculated excitation energy of 6.918 eV, is due to a transition from the 3a″ orbital into a pure d-type Rydberg orbital (Figure 4). At slightly higher excitation energies, states {8}, {9}, {11} and {13} also contain contributions due to transitions into d-type orbitals, together with valence contributions. Although the predicted excitation energies of these 3d states are a little lower than those of the absorption bands tentatively ascribed to the corresponding states in the experimental spectrum,

the theoretical results provide support for the proposed assignments. The excitation energies and proposed assignments of the vibrational structure associated with the Rydberg states marked in Figure 6 are listed in Table 3.

At energies above 7.6 eV, an examination of the vibrational structure appearing in the experimental spectrum suggests that the peaks at 7.681, 7.832 and 7.939 eV correspond to adiabatic transitions into Rydberg states. The resulting quantum defects are δ = 0.577, 0.330 and 0.118, respectively, if we assume that n = 4 in all these states. Our calculations predict that state {18}, with an excitation energy of 7.593 eV, arises from the $3a'' \rightarrow 4p_z$ A′ transition. Thus, state {18} belongs to the same Rydberg series as state {3}, which we have associated with the absorption bands observed between 6.2 and 6.9 eV (Figure 5(a)). Based on our theoretical results, and the derived quantum defect, the peak at 7.681 eV is ascribed to the adiabatic transition into the $4p_z$ A′ Rydberg state. The NTO plot for state {16} (Figure 4) indicates that it contains a contribution from excitation into a 4d orbital. Although the calculated transition energy for state {16} (and other nearby predominantly 4d states) are somewhat lower than that for the experimental peak at 7.939 eV, we nevertheless associate this peak with the adiabatic transition into a 4d orbital. The quantum defect for this peak suggests that it could be the n = 4 member of the same Rydberg series in which the peak at 7.326 eV corresponds to the n = 3 member. The assignment of the peak at 7.832 eV is more perplexing. The quantum defect of 0.330 suggests that the Rydberg state could be either p-type or d-type. However, all of the predicted states in the relevant energy range have a mixed Rydberg/valence character, so assignments based on quantum defect considerations may be unreliable.

A group of peaks having an average spacing of ~105 meV appears in the absorption spectrum between 9.2 and 9.8 eV (Figure 3(a)). This spacing is similar to the vibrational spacing (~108 meV) observed in the low binding energy region of the second photoelectron band of imidazole [13]. The term value of the structure observed in the absorption spectrum suggests that if it is associated with a Rydberg state belonging to a series converging onto the *A* state ionisation limit, then the principal quantum number of that state would be n = 5. The lower

members (n = 3, 4) of that series would probably be difficult to discern as they would be predicted to occur within the complex absorption band containing numerous Rydberg states belonging to series converging onto the $X\ ^2A''$ ionisation limit.

4.3. Photoabsorption spectrum of 1-methylimidazole

In general, the UV absorption spectrum of 1-methylimidazole (Figure 3(b)) resembles that of imidazole (Figure 3(a)) but with the corresponding features shifted to lower energy by ~0.18 eV. A similar shift to lower energy (~0.16 eV) is observed for the absorption bands due to valence transitions in toluene [30] compared to those in benzene [31]. This shift is a consequence of the electron-donating properties of the CH_3 substituent which tend to stabilise the molecular orbitals, thereby leading to lower excitation energies. Thus, it appears reasonable to anticipate that the structure observed in the absorption spectrum of 1-methylimidazole may be interpreted in a manner similar to that described for imidazole. The effects of the substituent on molecular excitation energies have been observed in many molecules [29,32]. In general, the raising or the lowering of the excitation energy in the substituted molecule, in relation to that in the unsubstituted molecule, depends upon the electron-withdrawing, or electron-donating, properties, respectively, of the substituent.

The assignment of the vibrational progressions associated with the absorption bands due to Rydberg states in 1-methylimidazole is hampered by the lack of a high-resolution photoelectron spectrum of the $(4a'')^{-1}\ X\ ^2A''$ state. Klasinc et al. [33] have recorded HeI excited photoelectron spectra of imidazole and several methylimidazoles and state that vibrational progressions involving the excitation of modes having energies of ~87, 130 and 175 meV can be observed, at high resolution, in the X state photoelectron bands of these compounds. An inspection of their published X state photoelectron band of 1-methylimdazole indicates that the main vibrational excitation involves the mode with an energy of ~170 meV. Klasinc et al. [33] quote a vertical ionisation energy of 8.69 eV which seems to correspond to the second peak in the X state band.

The threshold photoelectron spectrum of 1-methylimidazole recorded in the present study is plotted in Figure 7, together with the vertical ionisation energies (Table 4) calculated using the OVGF approach. In a conventional electron energy resolved photoelectron spectrum, such as a HeI excited spectrum, the signal arises predominantly through direct ionisation. In contrast, in a threshold photoelectron spectrum resonant autoionisation of neutral (mainly Rydberg) states can affect both the band profile and the relative intensity. These differences are apparent when comparing the present threshold photoelectron spectrum of 1-methylimidazole with the conventional, energy resolved, spectrum recorded by Klasinc et al. [33], and are typical of those observed in small polyatomic molecules [22,34,35].

The *X* state threshold photoelectron band exhibits a peak at 8.537 eV, attributed to the adiabatic ionisation energy, a shoulder at 8.664 eV, followed by another peak at 8.706 eV. The energy intervals between the shoulder and the peak due to the adiabatic transition, and between the first and second peaks, are 127 and 169 meV, respectively. We attribute the vibrational energy of 169 meV to the ν_9^+ mode, whose theoretically predicted energies in the neutral and ionic ground states are 175 and 172 meV, respectively (Table S2, Supplementary Information). The shoulder experimentally observed at 8.664 eV probably arises from excitation of the ν_{15}^+ and ν_{16}^+ modes. In the ground ionic state, the theoretically predicted vibrational energies of modes ν_{15}^+ and ν_{16}^+ are 131 and 122 meV, respectively. Below, we will use the complete listing of calculated vibrational energies for the neutral ground and *X* ionic states of 1-methylimidazole presented in Table S2 to help identify the vibrational structure associated with Rydberg states in the absorption spectra and to assign the excited modes.

According to our theoretical results for the excited electronic states of 1-methylimidazole (Table 2), the lowest lying state has a mixed valence (σ_{CH}) and Rydberg (3s) character, a transition energy of 5.664 eV and an oscillator strength of 0.0076. The threshold region of the absolute photoabsorption cross section of 1-methylimidazole is shown in Figure S1. A distinct onset is not evident in the experimental spectrum, with the absorption gradually

increasing from ~5.2 eV. Two very broad peaks are discernible around 5.69 and 5.83 eV (Figure 3(b)).

Figure 8 shows the photoabsorption spectrum of 1-methylimidazole in the energy range 6.0 – 6.8 eV. Inserting our experimental value of 8.537 eV for the adiabatic ionisation energy of 1-methylimidazole into Eq (2), results in a quantum defect of δ = 0.626 for the absorption band at 6.123 eV, assuming n = 3. A quantum defect of this value is typical of a p-type Rydberg state.

Our calculations predict that transitions from the outermost 4a″ orbital into the three Rydberg 3p orbitals fall within the lower energy portion of this range (Table 2). In each case, the excited orbital possesses a mixed Rydberg 3p and valence character. State {2}, with a calculated transition energy of 5.978 eV and a large oscillator strength of 0.122, has a mixed valence π^* and Rydberg $3p_z$ character, as is evident in the plot of the NTO (Figure 9). State {3}, having a less strongly mixed valence σ_{CH} and Rydberg $3p_{xy}$ character (Figure 9), has a smaller oscillator strength (0.0148) and a calculated transition energy of 6.212 eV. The oscillator strength of state {4}, having a mixed valence σ_{CH}^* and Rydberg $3p_{yx}$ character, is negligible (0.001).

Our simulation of the $X\,^2A''$ state photoelectron band of 1-methylimidazole is plotted in Figure 8 and broadly reproduces the main features occurring in the photoabsorption spectrum. Nevertheless, some discrepancies between the simulated and experimental spectra are evident, particularly around 6.2 eV. In view of these discrepancies, we offer two possible interpretations for the structure observed between 6.1 and 6.5 eV.

The first interpretation assumes that transitions into a single Rydberg state {2}, due to the 4a″ → $3p_z$ A′ excitation, dominate this region of the spectrum. The vibrational simulation suggests that peak C (Figure 8), observed at 6.293 eV, should be assigned to excitation of the ν_9 mode. Such an assignment results in a measured vibrational energy for this mode of 170 meV, in comparison with our calculated harmonic energies (scaled by a factor 0.97 as in Figure

4) of 175 and 172 meV, in the neutral and ionic ground states, respectively. Peak B (Figure 8), located at 6.202 eV in the experimental spectrum, with an experimental vibrational energy of 79 meV, might be due to excitation of mode $\nu_{19,}$ whose scaled calculated energy in the ionic ground state is 77 meV. Table 5 provides a summary of the assignments based upon this interpretation. The drawback with this interpretation is that there is little evidence, between peaks B and C in the experimental spectrum, of the peak predicted to arise from excitation of the ν_{15} and ν_{16} modes.

An alternative interpretation for the structure appearing between 6.1 and 6.5 eV involves transitions into two Rydberg states. The excitation energy for the $4a'' \rightarrow 3p_{xy}$ A'' transition is predicted to lie ~0.2 eV above that due to the $4a'' \rightarrow 3p_z$ A' transition (Table 2). The involvement of two Rydberg states ({2} and {3}) would allow the peak (B) at 6.202 eV to be attributed to the adiabatic transition into state {3}, with the peak (D) observed at 6.368 being assigned to excitation of the ν_9 mode. Table 5 also provides a summary of the assignments assuming that excitations into two Rydberg states give rise to the absorption bands. The advantage with the two-state interpretation is that most of the vibrational structure can be assigned to excitations involving the ν_9 mode, which our simulations indicate should be the most strongly excited mode. A high-resolution photoelectron spectrum of the *X* state of 1-methylimidazole is required to clarify the assignments proposed for the peaks observed in the absorption spectrum and to investigate the peak predicted to arise from excitation of the ν_{15}^+ and ν_{16}^+ modes in the simulated $X\ ^2A''$ state photoelectron spectrum.

The photoelectron band associated with the 18a′ orbital is broad and structureless [33]. Thus, the transition from the 18a′ orbital that has been ascribed to state {5} might be expected to result in a similarly structureless absorption band. The very broad feature appearing around 6.71 eV in the absorption spectrum might be associated with state {5}.

A prominent absorption band occurs in the experimental spectrum at 7.103 eV, followed by a doublet with peaks at 7.190 and 7.223 eV. It appears reasonable to ascribe the band at

7.103 eV as being due to the adiabatic transition into a Rydberg state. It also seems likely that the peaks at 7.190 and 7.223 eV arise from adiabatic transitions into Rydberg states. The energy intervals between these two peaks, and the peak at 7.103 eV, suggest that an alternative assignment as excited vibrational levels of the proposed Rydberg state having an origin at 7.103 eV seems less likely. The quantum defect for the band at 7.103 eV is –0.080, assuming $n = 3$.

Our theoretical results (Table 2) predict that state {6} (Figure 9), with a calculated transition energy of 6.690 eV and an oscillator strength of 0.0177, has a mixed valence π* and Rydberg 3d character, while state {7}, at 6.719 eV, has a pure Rydberg 3d character and significantly lower oscillator strength. Thus, it appears reasonable to ascribe the band observed at 7.103 eV to state {6}, whose Rydberg character is 3d.

States {8}, {9}, {10} and {14} all have a reasonably high calculated oscillator strength and the NTO plots for these states (only state {8} is shown in Figure 9) suggest that each possesses a pure Rydberg, or mixed valence/Rydberg character. It is difficult, nonetheless, to associate specific absorption bands with these states. The bands in the experimental spectrum are broad and do not appear to form regular Rydberg series, probably as a result of strong Rydberg/valence mixing.

5. Summary

The UV excited photoabsorption spectra of imidazole and 1-methylimidazole have been measured from threshold up to 10.8 eV. For each molecule, the spectrum exhibits several broad bands due to transitions into excited valence states and some sharp structure associated with Rydberg states. Assignments for some of the observed bands have been proposed using calculated transition energies and oscillator strengths. The NTO plots indicate that many of the electronically excited states have a mixed Rydberg/valence character.

Particular attention has been paid to the identification and assignment of absorption bands due to transitions into Rydberg states. For an unperturbed Rydberg state, the vibrational structure appearing in the photoelectron spectrum should be similar to that observed in the

photoelectron band associated with the ionic state onto which the Rydberg series converges. Moreover, the transition energies for unperturbed Rydberg states can be estimated using the Rydberg formula (Eq (2)), and the derived quantum defect may act as a guide to the identification of the excited state. Assignments based on quantum defect considerations become less reliable for states having a mixed Rydberg/valence character as the mixing may lead to transition energies shifted from those predicted by the Rydberg formula, and to irregular intensity distributions.

The absorption spectrum of imidazole exhibits several groups of peaks whose vibrational structure resembles that observed in the $X\,^2\mathrm{A}''$ state photoelectron band [13], thereby indicating that each group of peaks should be associated with a Rydberg state. In general, such assignments are supported by our calculated transition energies and oscillator strengths, and by the Rydberg character evident in the NTO plot. This procedure has resulted in a particularly satisfactory interpretation of the absorption bands observed in the energy range 6.2 – 6.9 eV, which appear to arise predominantly from the $3a'' \rightarrow 3p_z\ A'$ transition. At higher energy, some of the absorption bands have been assigned to transitions into 3d and 4p Rydberg states, based upon quantum defect considerations and calculated transition energies.

Assignments for the absorption bands observed in the spectrum of 1-methylimidazole have been hampered by the lack of a high-resolution photoelectron spectrum of the $X\,^2\mathrm{A}''$ state. Our simulations of the vibrational structure associated with this ionic state appear consistent with the reported experimental results [33] but a detailed comparison could not be made. The absorption spectrum of 1-methylimidazole exhibits several peaks in the energy range 6.1 – 6.5 eV which probably arise from excitations into one, or perhaps two, Rydberg states. Although our simulated vibrational spectrum reproduces some of the observed absorption structure, discrepancies are also apparent. This suggests that the absorption bands might arise from transitions into more than one Rydberg state. The confirmation of these proposed assignments requires further experimental work.

The NTO plots, in allowing the Rydberg/valence character of the excited states to be assessed, have contributed significantly to the understanding of the absorption spectra. Many of the excited states have a mixed character. The appearance of absorption bands typical of those expected for transitions into Rydberg states seems to correlate satisfactorily with the NTO plots indicating a substantial Rydberg contribution.

Disclosure Statement

The authors declare no conflict of interest.

Funding

D.M.P.H is grateful to the Science and Technology Facilities Council (United Kingdom) for financial support. The University of Nottingham High Performance Computing Facility provided computational resources supporting this investigation.

ORCID

David M P Holland http://orcid.org/0000-0003-1351-605X

David Townsend http://orcid.org/0000-0002-2522-4655

Ivan Powis http://orcid.org/0000-0002-7941-9079

References

[1] J. Del Bene and H. H. Jaffé, J. Chem. Phys. **48**, 4050 (1968).

[2] F. B. C. Machado and E. R. Davidson, J. Chem. Phys. **97**, 1881 (1992).

[3] L. Serrano-Andrés, M. P. Fülscher, B. O. Roos, and M. Merchán, J. Phys. Chem. **100**, 6484 (1996).

[4] M. Schreiber, M. R. Silva-Junior, S. P. A. Sauer, and W. Thiel, J. Chem. Phys. **128**, 134110 (2008).

[5] M. Barbatti, H. Lischka, S. Salzmann, and C. M. Marian, J. Chem. Phys. **130**, 034305 (2009).

[6] R. Crespo-Otero, M. Barbatti, H. Yu, N. L. Evans, and S. Ullrich, ChemPhysChem. **12**, 3365 (2011).

[7] A. L. Devine, B. Cronin, M. G. D. Nix, and M. N. R. Ashfold, J. Chem. Phys. **125**, 184302 (2006).

[8] P. E. Grebow and T. M. Hooker, Biopolymers **14**, 871 (1975).

[9] D. S. Caswell and T. G. Spiro, J. Am. Chem. Soc. **108**, 6470 (1986).

[10] W. Arbelo-González, R. Crespo-Otero, and M. Barbatti, J. Chem. Theory and Comput. 1**2**, 5037 (2016).

[11] D. J. Hadden, K. L. Wells, G. M. Roberts, L. T. Bergendahl, M. J. Paterson, and V. G. Stavros, Phys. Chem. Chem. Phys. **13**, 10342 (2011).

[12] H. Yu, N. L. Evans, V. G. Stavros, and S. Ullrich, Phys. Chem. Chem. Phys. **14**, 6266 (2012).

[13] M. Patanen, A. R. Abid, S. T. Pratt, A. Kivimäki, A. B. Trofimov, A. D. Skitnevskaya, E. K. Grigoricheva, E. V. Gromov, I. Powis, and D. M. P. Holland, J. Chem. Phys. **155**, 054304 (2021).

[14] R. L. Martin, J. Chem. Phys. **118**, 4775 (2003).

[15] F. Plasser, M. Wormit, and A. Dreuw, J. Chem. Phys. **141**, 024106 (2014)

[16] F. Plasser, S. A. Bäppler, M. Wormit, and A. Dreuw, J. Chem. Phys. **141**, 024107 (2014)

[17] D. M. P. Holland, D. A. Shaw, I. C. Walker, I. J. McEwen, and M. F. Guest, Chem. Phys. **344**, 227 (2008).

[18] D. M. P. Holland, Phys. Scripta **36**, 22 (1987).

[19] D. M. P. Holland, J. B. West, A. A. MacDowell, I. H. Munro, and A. G. Beckett, Nucl. Instrum. Methods Phys. Res. B **44**, 233 (1989).

[20] D. M. P. Holland, D. A. Shaw, S. Coriani, M. Stener, and P. Decleva, J. Phys. B **46**, 175103 (2013).

[21] D. M. P. Holland, D. A. Shaw, I. Sumner, M. A. Hayes, R. A. Mackie, B. Wannberg, L. G. Shpinkova, E. E. Rennie, L. Cooper, C. A. F. Johnson, and J. E. Parker, Nucl. Instrum. Methods Phys. Res. B **179**, 436 (2001).

[22] E. E. Rennie, L. Cooper, C. A. F. Johnson, J. E. Parker, R. A. Mackie, L. G. Shpinkova, D. M. P. Holland, D. A. Shaw, and M. A. Hayes, Chem. Phys. **263**, 149 (2001).

[23] M. J. Frisch, G. W. Trucks, H. B. Schlegel, G. E. Scuseria, M. A. Robb, J. R. Cheeseman, G. Scalmani, V. Barone, G. A. Petersson, H. Nakatsuji, X. Li, M. Caricato, A. V. Marenich, J. Bloino, B. G. Janesko, R. Gomperts, B. Mennucci, H. P. Hratchian, J. V. Ortiz, A. F. Izmaylov, J. L. Sonnenberg, D. Williams-Young, F. Ding, F. Lipparini, F. Egidi, J. Goings, B. Peng, A. Petrone, T. Henderson, D. Ranasinghe, V. G. Zakrzewski, J. Gao, N. Rega, G. Zheng, W. Liang, M. Hada, M. Ehara, K. Toyota, R. Fukuda, J. Hasegawa, M. Ishida, T. Nakajima, Y. Honda, O. Kitao, H. Nakai, T. Vreven, K. Throssell, J. J. A. Montgomery, J. E. Peralta, F. Ogliaro, M. Bearpark, J. J. Heyd, E. Brothers, K. N. Kudin, V. N. Staroverov, T. A. Keith, R. Kobayashi, J. Normand, K. Raghavachari, A. Rendell, J. C. Burant, S. S. Iyengar, J. Tomasi, M. Cossi, J. M. Millam, M. Klene, C. Adamo, R. Cammi, J. W. Ochterski, R. L. Martin, K. Morokuma, O. Farkas, J. B. Foresman, and D. J. Fox, Gaussian 16 Revision A.03 (Gaussian Inc., Wallingford, CT, 2016).

[24] Y. Shao, Z. Gan, E. Epifanovsky, A. T. B. Gilbert, M. Wormit, J. Kussmann, A. W. Lange, A. Behn, J. Deng, X. Feng, D. Ghosh, M. Goldey, P. R. Horn, L. D. Jacobson, I. Kaliman, R. Z. Khaliullin, T. Kuś, A. Landau, J. Liu, E. I. Proynov, Y. M. Rhee, R. M. Richard, M. A. Rohrdanz, R. P. Steele, E. J. Sundstrom, H. L. Woodcock, P. M. Zimmerman, D. Zuev, B. Albrecht, E. Alguire, B. Austin, G. J. O. Beran, Y. A. Bernard, E. Berquist, K. Brandhorst, K. B. Bravaya, S. T. Brown, D. Casanova, C.-M. Chang, Y.

Chen, S. H. Chien, K. D. Closser, D. L. Crittenden, M. Diedenhofen, R. A. DiStasio, H. Do, A. D. Dutoi, R. G. Edgar, S. Fatehi, L. Fusti-Molnar, A. Ghysels, A. Golubeva-Zadorozhnaya, J. Gomes, M. W. D. Hanson-Heine, P. H. P. Harbach, A. W. Hauser, E. G. Hohenstein, Z. C. Holden, T.-C. Jagau, H. Ji, B. Kaduk, K. Khistyaev, J. Kim, J. Kim, R. A. King, P. Klunzinger, D. Kosenkov, T. Kowalczyk, C. M. Krauter, K. U. Lao, A. D. Laurent, K. V. Lawler, S. V. Levchenko, C. Y. Lin, F. Liu, E. Livshits, R. C. Lochan, A. Luenser, P. Manohar, S. F. Manzer, S.-P. Mao, N. Mardirossian, A. V. Marenich, S. A. Maurer, N. J. Mayhall, E. Neuscamman, C. M. Oana, R. Olivares-Amaya, D. P. O'Neill, J. A. Parkhill, T. M. Perrine, R. Peverati, A. Prociuk, D. R. Rehn, E. Rosta, N. J. Russ, S. M. Sharada, S. Sharma, D. W. Small, A. Sodt, T. Stein, D. Stück, Y.-C. Su, A. J. W. Thom, T. Tsuchimochi, V. Vanovschi, L. Vogt, O. Vydrov, T. Wang, M. A. Watson, J. Wenzel, A. White, C. F. Williams, J. Yang, S. Yeganeh, S. R. Yost, Z.-Q. You, I. Y. Zhang, X. Zhang, Y. Zhao, B. R. Brooks, G. K. L. Chan, D. M. Chipman, C. J. Cramer, W. A. Goddard, M. S. Gordon, W. J. Hehre, A. Klamt, H. F. Schaefer, M. W. Schmidt, C. D. Sherrill, D. G. Truhlar, A. Warshel, X. Xu, A. Aspuru-Guzik, R. Baer, A. T. Bell, N. A. Besley, J.-D. Chai, A. Dreuw, B. D. Dunietz, T. R. Furlani, S. R. Gwaltney, C.-P. Hsu, Y. Jung, J. Kong, D. S. Lambrecht, W. Liang, C. Ochsenfeld, V. A. Rassolov, L. V. Slipchenko, J. E. Subotnik, T. Van Voorhis, J. M. Herbert, A. I. Krylov, P. M. W. Gill and M. Head-Gordon, Mol. Phys. 113, 184 (2015).

[25] K. Kaufmann, W. Baumeister, and M. Jungen, J. Phys. B **22**, 2223 (1989).

[26] G. Herzberg, *Molecular Spectra and Molecular Structure II: Infrared and Raman Spectra of Polyatomic Molecules* (Van Nostrand Reinhold, New York, 1945).

[27] J. P. Merrick, D. Moran, and L. Radom, J. Phys. Chem. A **111**, 11683 (2007).

[28] M. Majoube and G. Vergoten, J. Mol. Struct. **266**, 345 (1992).

[29] M. B. Robin, *Higher Excited States of Polyatomic Molecules*, vol. 1 (Academic Press, New York, 1974).

[30] C. Serralheiro, D. Duflot, F. Ferreira da Silva, S. V. Hoffmann, N. C. Jones, N. J. Mason, B. Mendes, and P. Limäo-Vieira, J. Phys. Chem. A 1**19**, 9059 (2015).

[31] F. J. Capalbo, Y. Bénilan, N. Fray, M. Schwell, N. Champion, Et. Es-sebbar, T. T. Koskinen, I. Lehocki, and R. V. Yelle, Icarus **265**, 95 (2016).

[32] M. B. Robin, *Higher Excited States of Polyatomic Molecules*, vol. 2 (Academic Press, New York, 1974).

[33] L. Klasinc, B. Ruščić, F. Kajfež, and V. Šunjić, Int. J. Quantum. Chem. **14**(S5), 367, (1978).

[34] A.-M. Boulanger, E. E. Rennie, D. M. P. Holland, D. A. Shaw, and P. M. Mayer, J. Phys. Chem. A **110**, 8563 (2006).

[35] D. M. P. Holland, D. A. Shaw, M. Stener, and P. Decleva, J. Phys. B **42**, 245201 (2009).

Tables

Table 1

TD-DFT CAM-B3LYP/d-Aug-cc-pVTZ calculations of vertical excitation energies, oscillator strengths, and spatial extents for singlet excited states of imidazole.

State		Energy (eV)	Oscillator Strength *f*	Excited State Spatial Properties [a]			Natural Transition Orbitals	
No.	Symmetry			$\Delta\langle R_\chi^2\rangle$ (a.u.) [b]	R_e (Å)	$D_{e\text{-}h}$ (Å)	Initial	Final [c]
20	A″	7.616	0.0009	7.9	2.2	2.8	15a′	π^*
19	A″	7.596	0.0009	185.0	10.7	10.8	3a″	d
18	A′	7.593	0.0082	321.0	7.8	8.1	3a″	$4p_z$
17	A″	7.438	0.0002	284.7	9.8	10.0	3a″	d
16	A′	7.376	0.0014	114.9	6.4	6.6	3a″	4d [π^*]
15	A″	7.348	0.0009	297.0	9.2	10.0	3a″	$4p_x$
14	A′	7.229	0.0031	118.8	6.4	6.6	3a″	4d
13	A″	7.189	0.0021	172.3	7.0	7.2	3a″	d
12	A′	7.147	0.0421	45.1	3.9	4.7	15a′	4s [σ_{NH}^*]
11	A″	7.142	0.0007	175.4	7.3	8.2	3a″	d/4s
10	A″	7.052	0.0027	59.4	4.2	4.8	2a″	s/(d) [σ_{NH}^*]
9	A″	6.982	0.0001	94.4	5.7	5.8	3a″	d [$\sigma_{NH}^*/\sigma_{CH}^*$]
8	A′	6.962	0.0342	25.0	3.2	3.6	3a″	d $\pi_{C\text{-}C\text{-}N}^*$
7	A″	6.918	0.0016	71.4	5.0	5.2	3a″	d
6	A′	6.745	0.0284	50.9	4.2	4.5	3a″	$3p_z$ [$\pi_{C\text{-}N\text{-}C=N}^*$]
5	A″	6.702	0.0039	3.6	1.9	2.5	15a′	$\pi_{C\text{-}N\text{-}C=N}^*$
4	A″	6.493	0.0005	70.8	4.9	5.2	3a″	$3p_y$ [σ_{CH}^*]
3	A′	6.267	0.1415	31.6	3.5	3.8	3a″	$3p_z$ $\pi_{C\text{-}C\text{-}N}^*$
2	A″	6.259	0.0241	65.7	4.4	4.9	3a″	$3p_x$ [σ_{CH}^* /σ_{NH}^*]
1	A″	5.515	0.0007	1.4	3.3	4.3	3a″	3s [σ_{NH}^*]

[a] These are: $\langle R_\chi^2\rangle$ - spatial extent of state (2nd moment of the electron density); R_e – electron size; $D_{e\text{-}h}$ – electron-hole separation. Both of the latter properties were obtained from the OPDM analysis.

[b] Relative to the ground state value of $\langle R_\chi^2\rangle$ = 284.7 a.u.

[c] Excited state character denoted, as appropriate, in terms of Rydberg and valence contributions. Relatively weak contributions to the overall final state character are denoted by inclusion within square brackets [].

Table 2

TD-DFT CAM-B3LYP/d-Aug-cc-pVTZ calculations of vertical excitation energies, oscillator strengths, and spatial extents for singlet excited states of 1-methylimidazole.

State		Energy (eV)	Oscillator Strength *f*	Excited State Spatial Properties [(a)]			Natural Transition Orbitals	
No.	Symmetry			$\Delta\langle R_\chi^2\rangle$ (a.u.) [(b)]	R_e (Å)	$D_{e\text{-}h}$ (Å)	Initial	Final [(c)]
15	A′	7.190	0.0167	49.0	4.4	4.9	18a′	s
14	A′	7.116	0.0443	101.2	6.1	6.4	4a″	p/d ? [[π*]]
13	A″	7.116	0.0001	207.5	8.0	8.4	4a″	d/p ? [[σ_{CH}]]
12	A′	7.064	0.0122	143.4	6.8	7.3	4a″	d
11	A″	7.025	0.0017	151.1	7.1	7.4	4a″	d
10	A″	6.913	0.0049	65.0	4.6	5.3	3a″	s [σ_{CH3}]
9	A″	6.851	0.0068	104.0	5.9	6.3	4a″	3d
8	A′	6.793	0.0191	86.0	5.4	5.6	4a″	$4p_z$ [π*]
7	A″	6.719	0.0023	67.9	4.9	5.3	4a″	3d
6	A′	6.690	0.0177	22.3	3.2	3.6	4a″	3d π*
5	A″	6.620	0.0024	4.6	2.3	2.9	18a′	$3p_z$ π*
4	A″	6.409	0.0010	79.1	5.2	5.6	4a″	$3p_{yx}$ [σ_{CH}*]
3	A″	6.212	0.0148	70.3	5.0	5.3	4a″	$3p_{xy}$ [σ_{CH}]
2	A′	5.978	0.1218	26.6	3.4	3.9	4a″	$3p_z$ π*
1	A″	5.664	0.0076	45.2	4.0	4.6	4a″	3s [σ_{CH}]

[(a)]These are: $\langle R_\chi^2\rangle$ - spatial extent of state (2nd moment of the electron density); R_e – electron size; $D_{e\text{-}h}$ – electron-hole separation. Both of the latter properties were obtained from the OPDM analysis.

[(b)]Relative to the ground state value of $\langle R_\chi^2\rangle$ = 490.4 a.u.

[(c)]Excited state character denoted, as appropriate, in terms of Rydberg and valence contributions. Relatively weak contributions to the overall final state character are denoted by inclusion within square brackets [].

Table 3

Proposed assignments and excitation energies of structure observed in the photoabsorption spectrum of imidazole

Proposed assignment		Excitation energy (eV)	Proposed assignment		Excitation energy (eV)
$3a''\rightarrow 3p_z$ A′	0^0	6.258	$3a''\rightarrow 3d$	0^0	7.416
	14^1	6.371		14^1?	7.523
	12^1	6.387		12^1	7.541
	7^1	6.427		7^1	7.581
	$7^1 14^1$	6.540	$3a''\rightarrow 4p$	0^0	7.681
	$7^1 12^2$	6.557		14^1	7.794
	7^2	6.593		12^1	7.811
	$7^2 14^1$	6.709		7^1	7.85
$3a''\rightarrow 3d$	0^0	7.326	$3a''\rightarrow 3d/4p$	0^0	7.832
	14^1	7.438		12^1	7.958
	12^1	7.454		7^1?	7.980
	7^1	7.498	$3a''\rightarrow 4d$	0^0	7.939
				14^1	8.053
				12^1	8.067
				7^1	8.111

Table 4

Ionisation energies of 1-methylimidazole calculated using the Outer Valence Green's Function method.

Orbital	Ionisation energy (eV)
13a′	17.702
1a″	16.090
14a′	15.584
15a′	14.558
16a′	14.385
17a′	13.919
2a″	13.766
18a′	10.072
3a″	9.712
4a″	8.602

Table 5

Proposed assignments and excitation energies of structure observed in the photoabsorption spectrum of 1-methylimidazole. Assignments are given for transitions into one ($3p_z$ A′) or, alternatively, two ($3p_z$ A′ and $3p_{xy}$ A″) Rydberg states.

Peak		Proposed assignment	
Label	Excitation energy (eV)	One Rydberg state	Two Rydberg states
A	6.123	$4a''\rightarrow 3p_z$ A′ 0^0	$4a''\rightarrow 3p_z$ A′ 0^0
B	6.202	$4a''\rightarrow 3p_z$ A′ 19^1	$4a''\rightarrow 3p_{xy}$ A″ 0^0
C	6.293	$4a''\rightarrow 3p_z$ A′ 9^1	$4a''\rightarrow 3p_z$ A′ 9^1
D	6.368	$4a''\rightarrow 3p_z$ A′ $9^1 19^1$	$4a''\rightarrow 3p_{xy}$ A″ 9^1
E	6.425	$4a''\rightarrow 3p_z$ A′ $9^1 15^1 + 9^1 16^1$	$4a''\rightarrow 3p_z$ A′ $9^1 15^1 + 9^1 16^1$
F	6.465	$4a''\rightarrow 3p_z$ A′ 9^2	$4a''\rightarrow 3p_z$ A′ 9^2

Figures

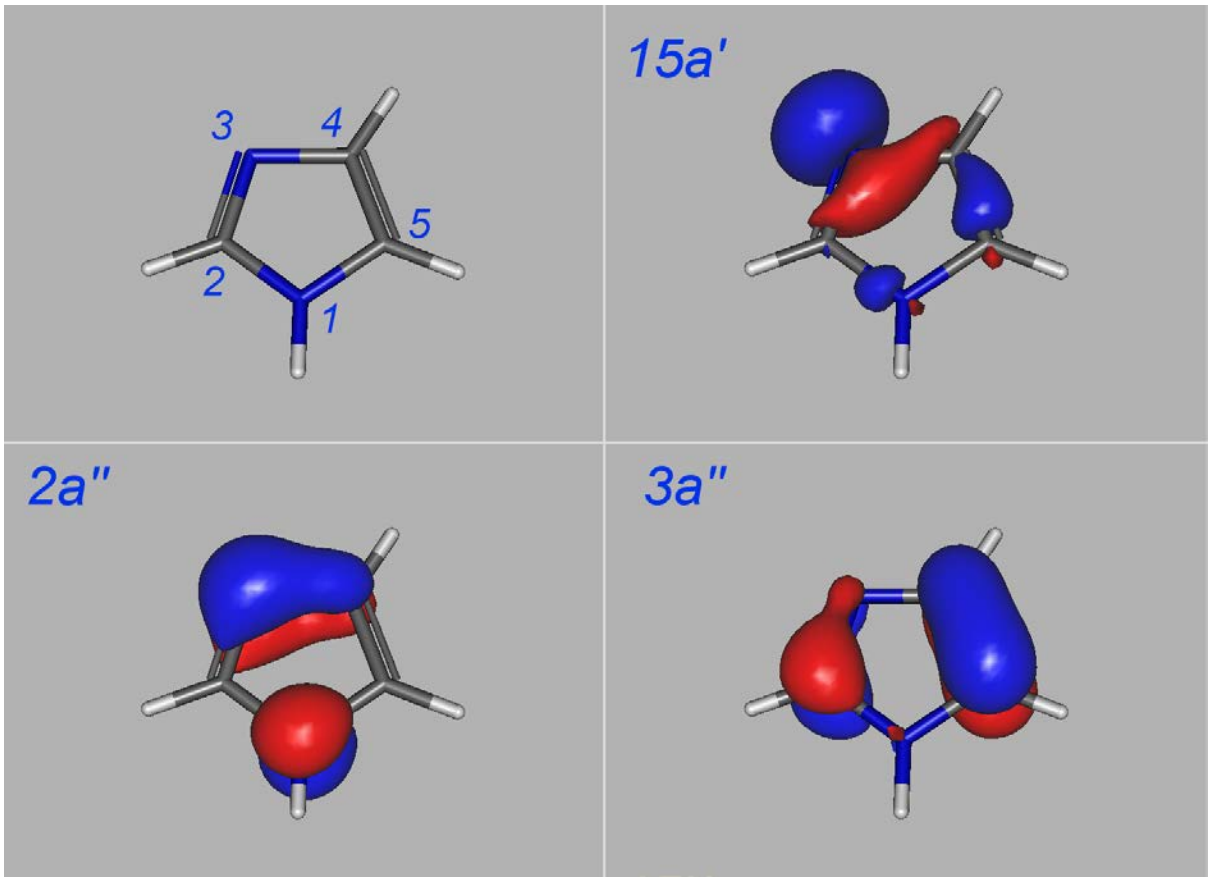

Figure 1

The three outermost molecular orbitals of imidazole (iso-surface Hartree-Fock density plots). The top left panel indicates the molecular orientation used for these plots and the atomic numbering. The nitrogen, carbon, and hydrogen atoms are coded blue, grey, and white, respectively.

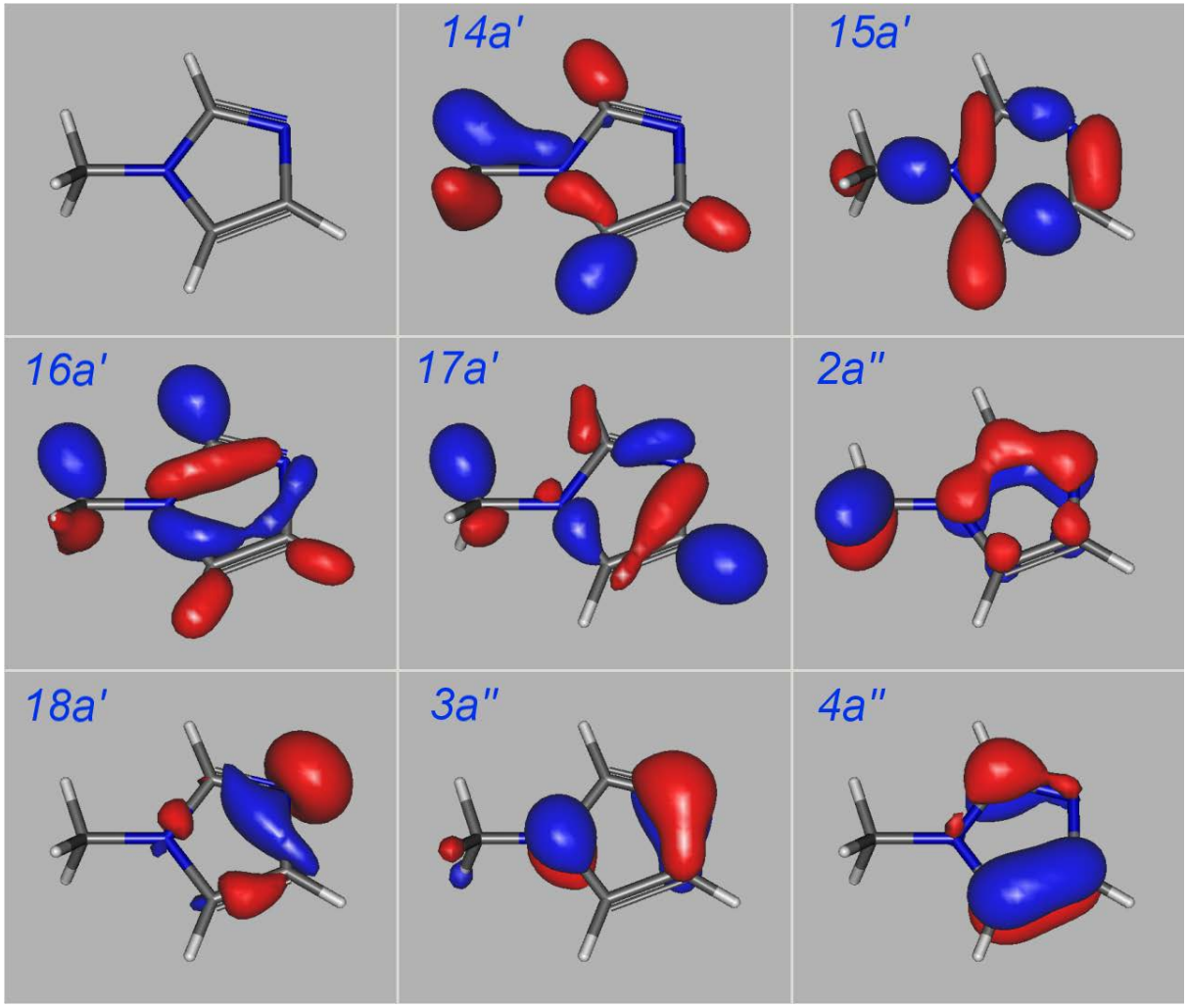

Figure 2

The outer valence molecular orbitals of 1-methylimidazole (iso-surface Hartree-Fock density plots). The top left panel indicates the molecular orientation used for these plots. The nitrogen, carbon, and hydrogen atoms are coded blue, grey, and white, respectively

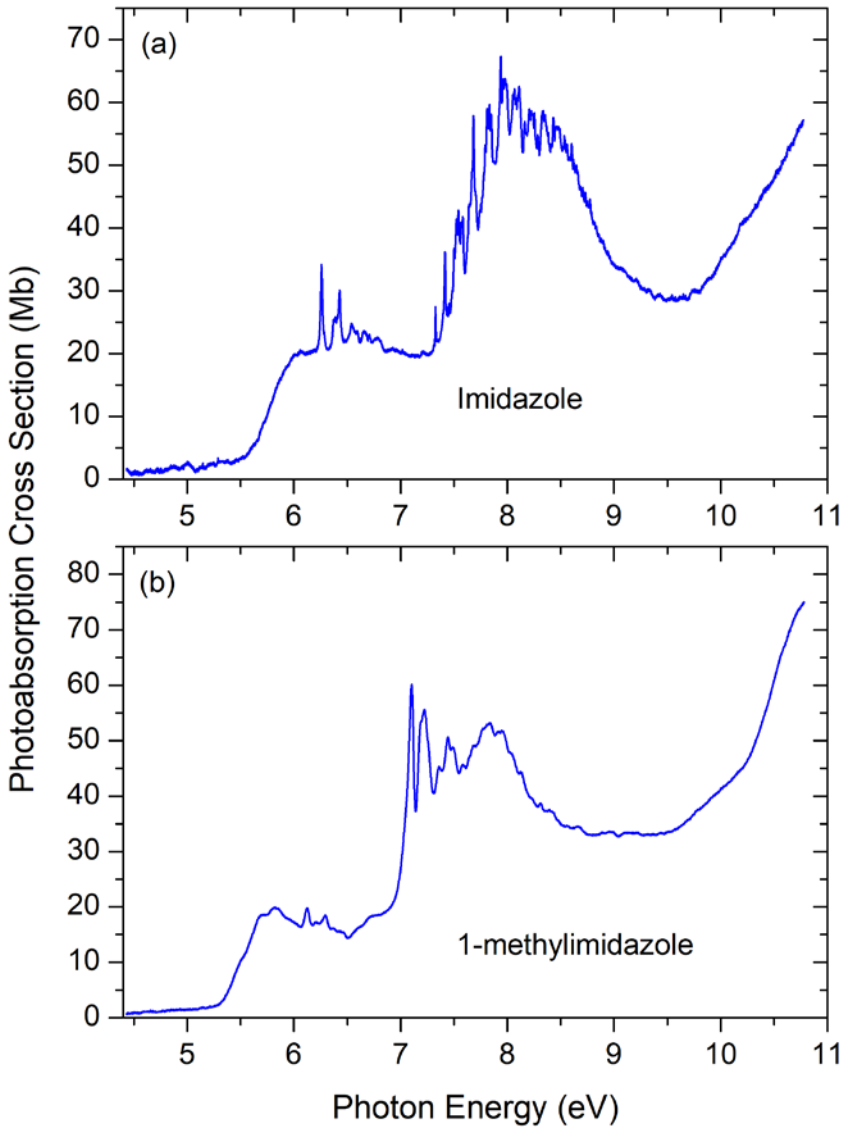

Figure 3

The absolute photoabsorption cross section of imidazole (a), and 1-methylimidazole (b).

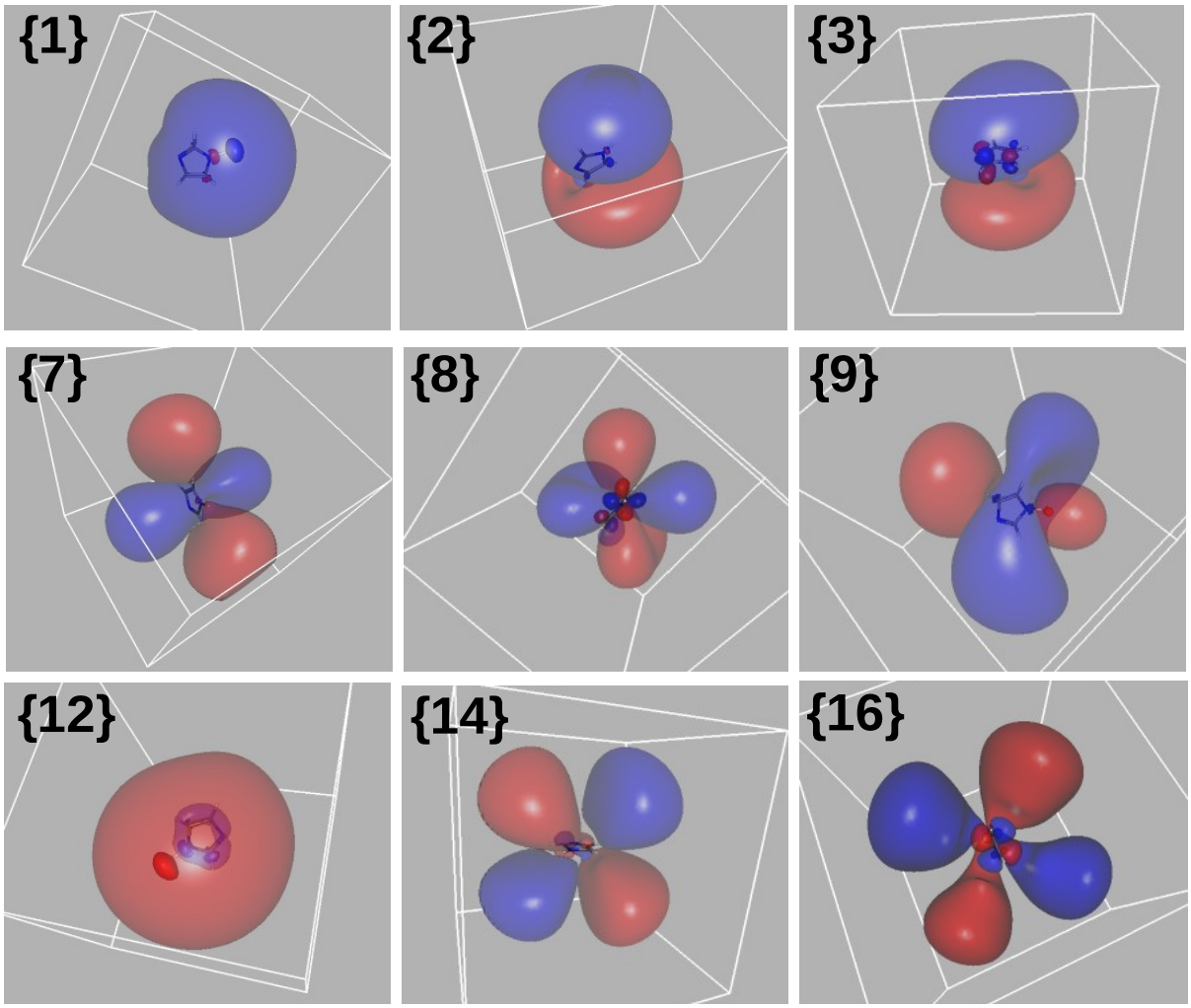

Figure 4

Selected excited NTO iso-surface density plots for imidazole. Electron density concentrations in the molecular core region are represented (when they exist) by a solid (opaque) surface with an iso value of ~0.05, typical of valence electron density. At longer range an outer (transparent) surface is drawn with a smaller iso value of 0.005 to capture the diffuse Rydberg character. These plots may be compared with the Rydberg/valence character noted in Table 1. For states {1} to {3}, the bounding box dimensions are set at ±14 a.u. along each edge, increasing to ±16 a.u for {7},{8} & {12}, and ± 18 a.u. for {9}, {14} & {16}. Notice the relatively greater valence density for states {3} and {8}. State {14} has an imperceptible core-region valence intensity, while state {16} has a clear π* valence contribution. For both of these states ({14} and {16}), the 4d orbital's radial node pattern is clearly evident in the outer, transparent, iso-surface plot near the molecular interior. Similar Rydberg *and* valence structure is seen in state {1} ($3a'' \rightarrow 3s/[\sigma_{NH}^*]$) and state {12} ($15a' \rightarrow 4s/[\sigma_{NH}^*]$).

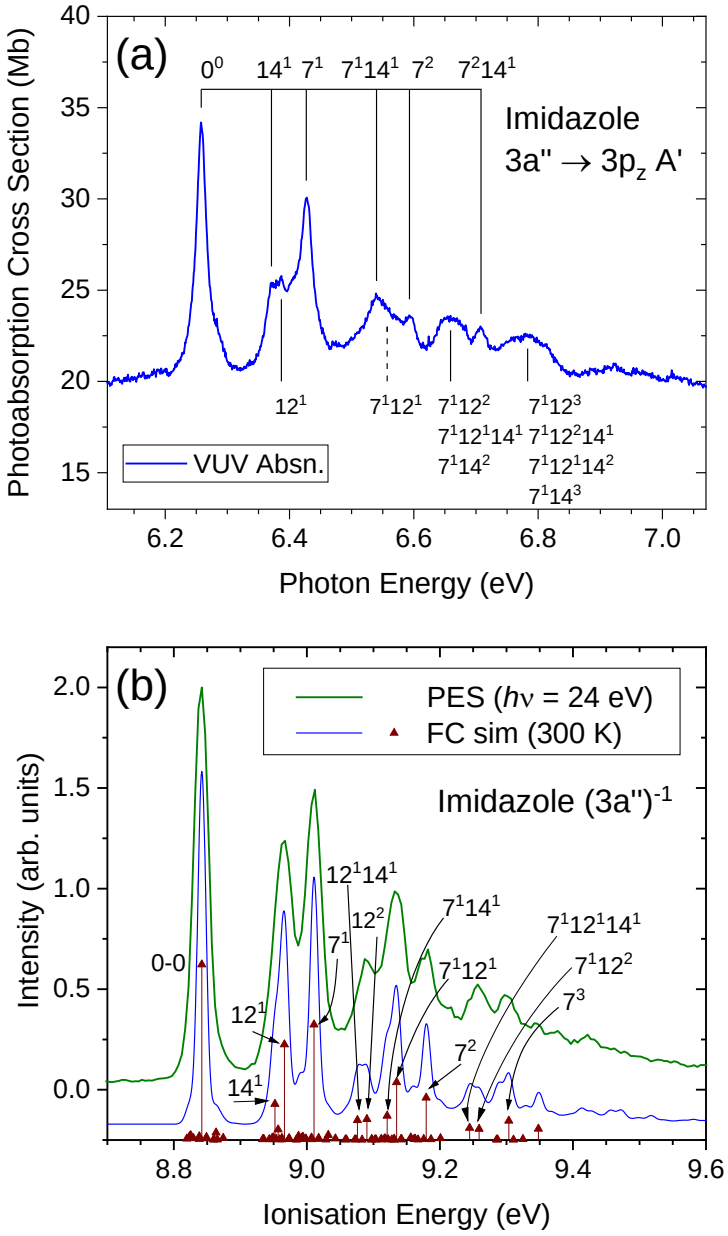

Figure 5

(a)The photoabsorption spectrum of imidazole in the photon energy range containing structure due to the 3a″ → 3p$_z$ A′ transition. (b)The $X\ ^2$A″ state photoelectron spectrum (PES) of imidazole recorded using a photon energy of 24 eV, and a 300 K Franck-Condon (FC) simulated spectrum with the calculated B3LYP/cc-pVTZ harmonic frequencies scaled by a factor of 0.97 (reproduced from Patanen et al. [13]).

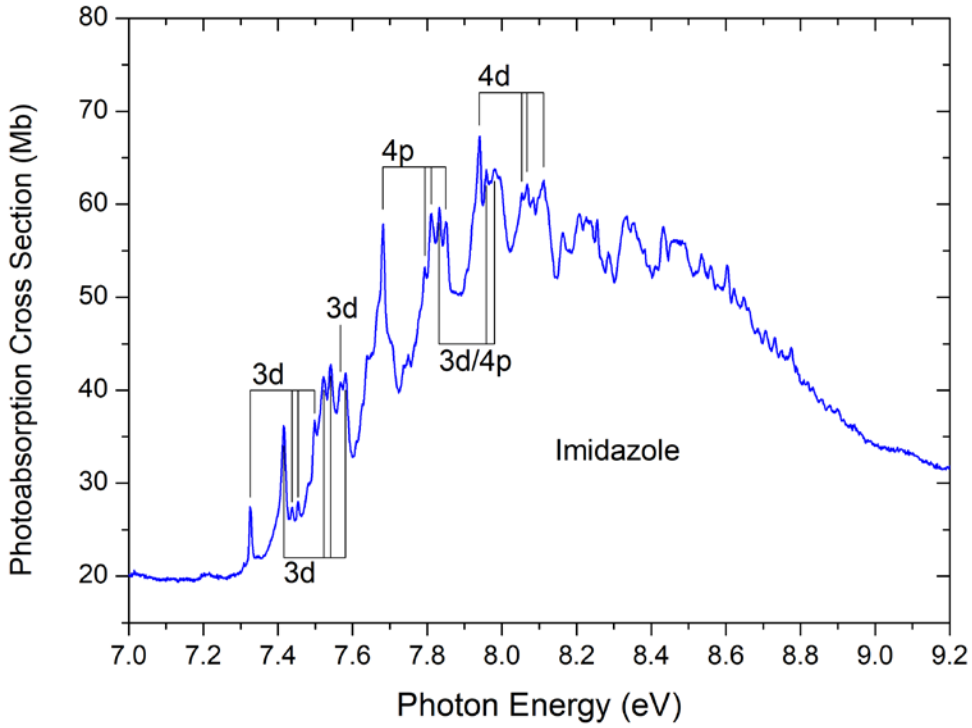

Figure 6

The absolute photoabsorption cross section of imidazole. Absorption bands tentatively assigned to transitions into the 3d, 4p or 4d Rydberg states are marked. The excitation energies of these transitions are given in Table 3.

.

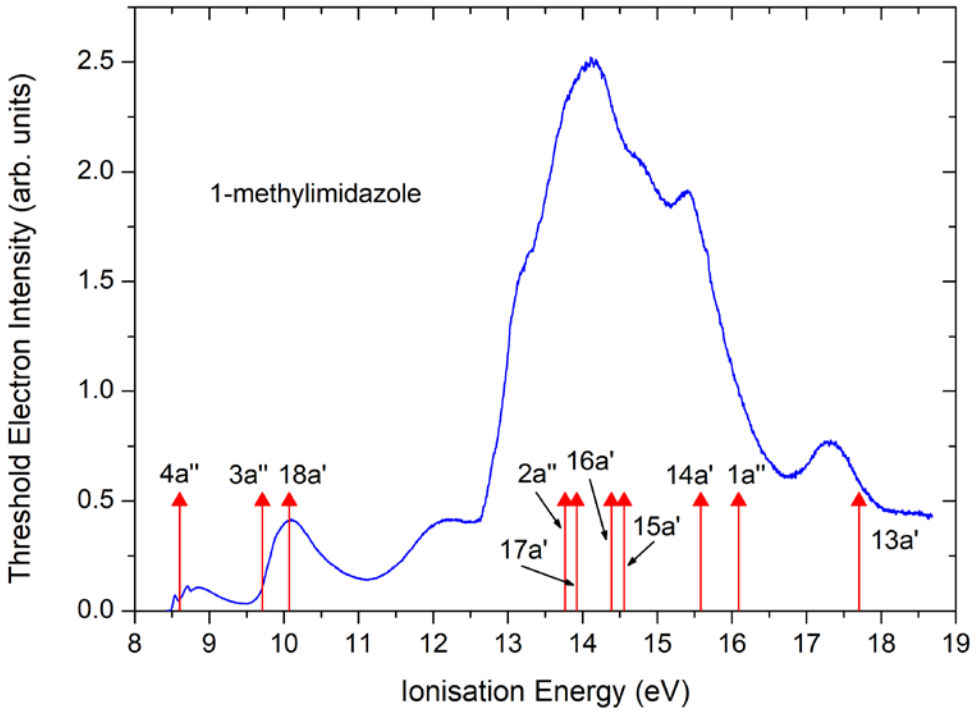

Figure 7

The valence shell threshold photoelectron spectrum of 1-methylimidazole. The OVGF ionisation energies (Table 4) are marked.

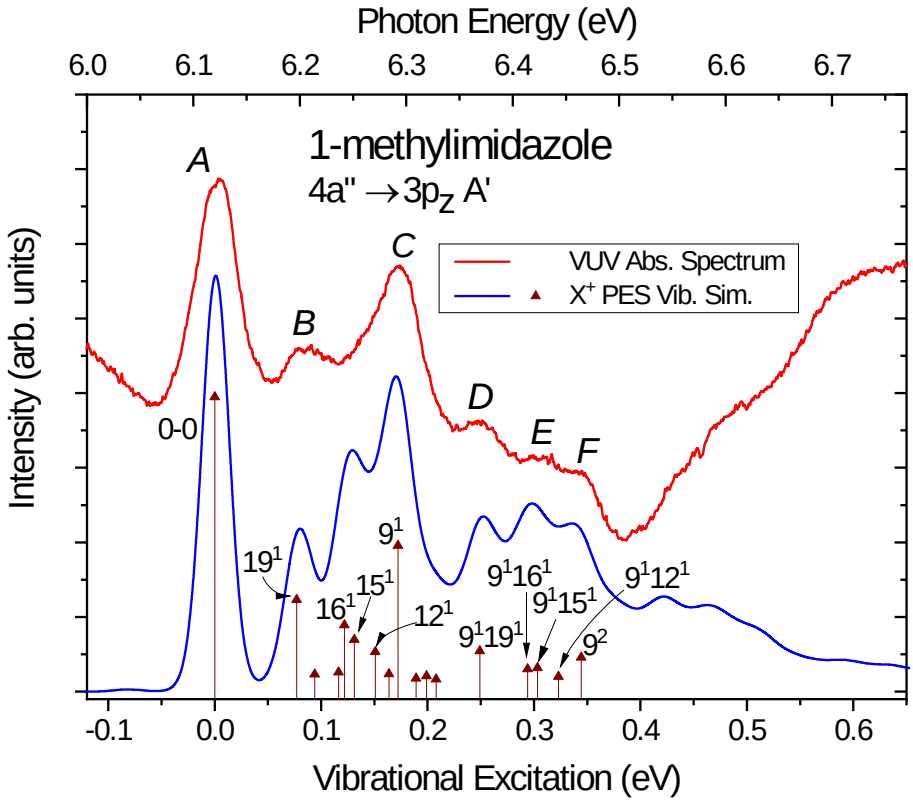

Figure 8

The photoabsorption spectrum of 1-methylimidazole in the 6 eV region, and a 300 K Franck-Condon simulation for the cation $X^+\ ^2A''$ state photoelectron spectrum, aligned to the origin (peak A) of the experimental absorption spectrum. The simulation uses B3LYP/cc-pVTZ harmonic analyses for the ground state neutral and cation vibrational modes (Table S2) with frequencies scaled by a factor 0.97 to improve correspondence with the experimental VUV absorption peak positions. Only the most intense transitions from the vibrationless ground state are shown as a stick spectrum, but all calculated transitions, including hot bands, have been convoluted with a Gaussian function of 240 cm^{-1} to generate a more realistic profile (blue line).

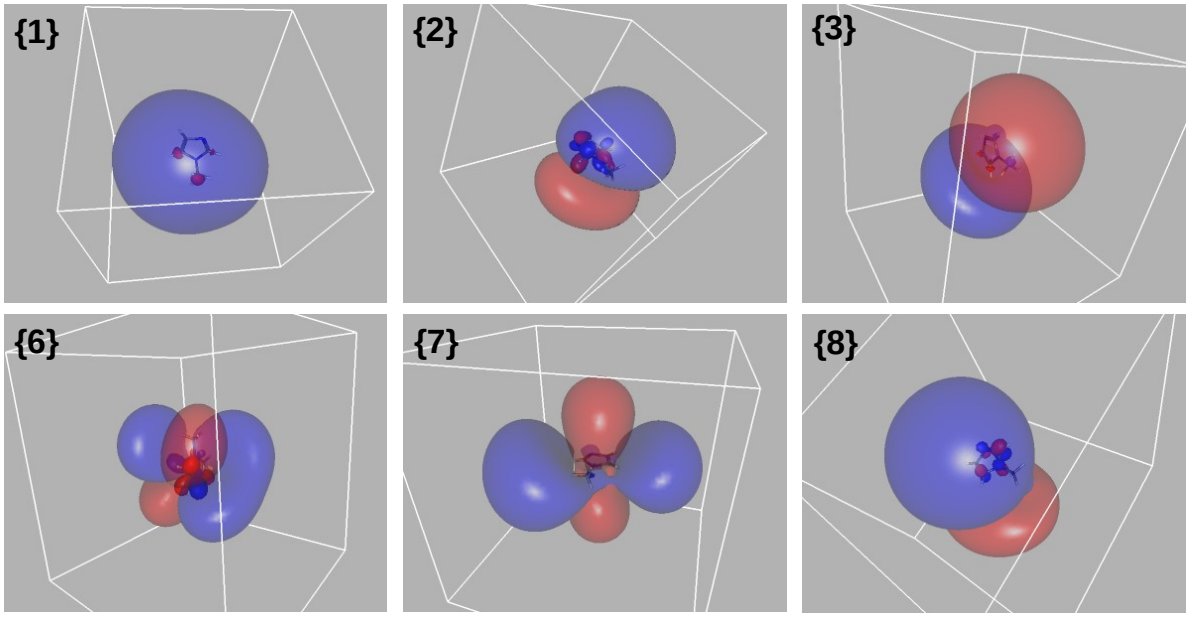

Figure 9

Examples of the excited NTO iso-surface density plots for 1-methylimidazole. A general explanation of these plots follows that accompanying Figure 4. The opaque interior surfaces (revealing valence structure) were constructed with iso-surface values of 0.04, and the transparent outer surfaces to examine the diffuse Rydberg structure were drawn for iso values of 0.005. The bounding boxes have edges that range ±15 a.u. for states {1} and {2}, increased to ±18 a.u. for the remainder shown here. The visual impression may be compared with the excited state characterisation listed for 1-methylimidazole in Table 2.